1 2 3 4

Package-less liquid phase sensing using surface acoustic waves on lithium tantalate oxide

David Rabus, Lilia Arapan, Jean-Michel Friedt, Vincent Luzet, and Frédéric Chérioux

***Abstract*— Surface acoustic wave transducers propagating shear waves are compatible with sensing chemical compounds in a liquid phase. However, if the liquid surrounding the sensor possesses a higher permittivity than the piezoelectric substrate, then the interdigitated electrodes for converting the incoming electromagnetic wave to acoustic waves is susceptible to capacitive short-circuiting, leading to excessive insertion losses. By using high-permittivity lithium tantalate oxide, we demonstrate chemical sensing in water without the need for dedicated microfluidic packaging. Nevertheless, the gravimetric sensitivity of these package-less transmission Love mode delay lines remains comparable to that of low-permittivity quartz when appropriately tuning the guiding layer thin film to confine energy to the surface in a Love mode. We extend the transmission line gravimetric sensitivity measurement to a reflective delay line geometry for passive transducers that can be wirelessly probed. For instance, Ground Penetrating RADAR can be used for sub-surface sensing, here targeting water pollution detection, operating in the 100 to 500 MHz range. This center frequency was selected as a tradeoff between penetration depth (lower frequency) and antenna size (smaller at higher frequency). Non specific binding of proteins detection is shown in the context of biosensing applications.**

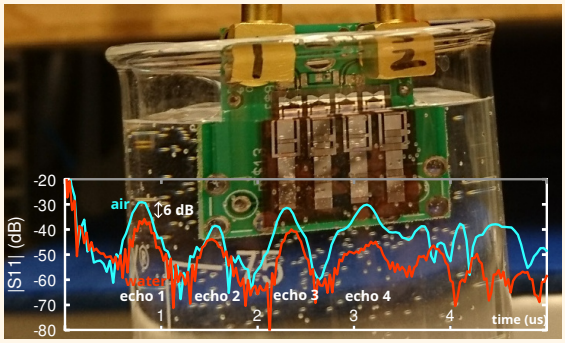

***Index Terms*— Surface acoustic wave, lithium tantalate oxide, gravimetric sensor, fluidics, reflective delay line, wireless**

I. Introduction

ACOUSTIC transducers are widely used as gravimetric sensors due to, on the one hand, the robust architecture and probing electronics, and on the other hand, the strong dependence of their characteristics with boundary conditions, whether in a bulk acoustic resonator architecture (so-called Quartz Crystal Micro-balance — QCM) or Surface Acoustic Wave (SAW) device [1]. The latter architecture is most commonly implemented using quartz, enabling the generation of a shear acoustic wave that experiences minimal attenuation when propagating over a surface covered with liquid. The sensing area along the propagation path is situated, in a transmission delay line configuration, between two Interdigitated Electrode Transducers (IDTs). The IDTs serve the dual purpose of converting incoming electromagnetic waves into acoustic waves through the inverse piezoelectric effect and converting acoustic waves back into electrical signals through the direct piezoelectric effect.

However, employing a low-permittivity quartz substrate presents a significant challenge: the capacitive short-circuiting of IDTs when covered with high-permittivity aqueous liquid. In such a setup, the electric field preferentially leaks into the water rather than into the piezoelectric substrate, resulting in unacceptable insertion losses that hinder accurate measurements of acoustic velocity, particularly for chemical binding events.

Numerous attempts have been made to prevent water from reaching the IDTs [2]–[4], but these efforts have been plagued by unreliable packaging solutions. This issue arises because the mechanical structures designed to shield the IDTs from liquid intrusion while permitting the detection of the compounds in this same liquid must be situated along the acoustic path. Striking the delicate balance between maintaining a tight seal and minimizing acoustic losses proves to be challenging, particularly in the context of reproducible cleanroom automated batch manufacturing [5]–[7].

Unlike the QCM architecture, where acoustic energy is confined to the center electrode and dissipates around the piezoelectric disc's periphery, allowing for the use of an O-ring seal to confine liquid without affecting acoustic characteristics, the microfluidic confinement system for SAW architecture must be positioned along the acoustic path. Consequently,

This work was supported in part by the French National Research Agency under grant UNDERGROUND ANR-17-CE24-0037 and by the TotalEnergies company. We also acknowledge partial support of the French RENATECH network and its FEMTO-ST technological facility (corresponding e-mail: jmfriedt@femto-st.fr)

All authors are affiliated with the FEMTO-ST Institute, Besançon, France

D. R. is now with Statice SAS, 25000 Besançon, France (e-mail: david.rabus@femto-st.fr).

L. A. is now with Silmach SA, 25000 Besançon, France (e-mail: lilia.arapan@femto-st.fr).

a SAW packageless (bio)chemical sensing solution becomes highly desirable.

The root cause of the capacitive short circuit, owing to the low permittivity of the substrate, suggests that opting for a high permittivity piezoelectric substrate could offer a viable solution. Lithium niobate oxide and lithium tantalate oxide (LTO) are both potential substrates, with lithium niobate being ruled out due to the absence of pure shear waves -— aside from the compression wave -— resulting in suboptimal gravimetric sensitivity [8].

The propagation of a shear wave not only prevents the dissipation of energy into the liquid and minimizes losses due to boundary condition mismatch but also facilitates the conversion into a Love mode SAW. This conversion enhances gravimetric sensitivity by confining acoustic energy to the surface [9], [10]. Achieving this confinement involves utilizing a thin guiding layer with a lower acoustic velocity than the SAW velocity within the piezoelectric substrate [11], [12].

While the Love mode conversion has been extensively studied in quartz, our focus here centers on the gravimetric sensitivity of Love-mode propagation on LTO.

The objective of the work is to provide a transducer suitable for detecting chemical compounds in water. We have identified two main application fields: the detection of biological compounds (biosensors) in water and of pollutant in groundwater. For the sensor operation not to be limited by an energy source, we furthermore aim at developing a passive transducer compatible with commercial, off the shelf sub-surface characterization geophysical instruments, Ground Penetrating RADARs (GPR). We have designed acoustic sensors meeting the requirements of both applications, and are not aware of any other technology able to meet these two requirements. Indeed, while the QCM [13] was established as the standard for biosensing using acoustic devices, their high-frequency (HF – 3-30 MHz) operating frequency makes them unsuitable for wireless interrogation due to the excessively large antenna size that would be needed to collect the probing radiofrequency wave. High-overtone Bulk Acoustic Resonators (HBAR) could be an alternative meeting both compatibility to liquid phase measurement without microfluidic packaging of the sensing area and very-high radiofrequency (VHF – 30-300 MHz) operation, but they have been demonstrated to only exhibit a gravimetric sensitivity determined by the fundamental mode [14], much lower than those achieved with SAW as demonstrated again in this investigation. High-fundamental Frequency QCM (HFF-QCM [15]) is yet another alternative but their thin suspended membrane makes them fragile and sensitive to hydrostatic pressure, an uncontrolled parameter if monitoring pollutants in the water table. On the other hand, optical measurement methods, either in a guided medium such as Surface Plasmon Resonance (SPR) or optical waveguides, or propagating in free space [16], would not be compatible with wireless sub-surface measurements, although optical fibers are becoming popular for densely distributed sub-surface arrays when measuring temperature, stress [17] or even chemical compounds [18].

The article is organized as follows: First, we employ numerical analysis to model the behavior of shear wave velocity from the free surface to a surface coated with a polymer. Next, we explore a transmission delay line architecture based on the selected substrate, which is coated with various organic layers of varying thicknesses to assess Love mode gravimetric sensitivity. Subsequently, we present a reflective delay line architecture designed for wireless measurement of the backscattered signal. Finally, we conclude our investigation with an experimental demonstration of the reflective delay line biosensing capability, all without requiring any dedicated microfluidics.

II. Acoustic propagation modeling

It is well known that LTO generates a strongly coupled Rayleigh wave and a pseudo-shear wave when using the YXl/36° cut [19]. However, the pseudo-shear wave is poorly confined to the surface. To prevent radiation into the bulk, either the acoustic path can be metallized to slow down the velocity below the bulk mode velocity, or a guiding layer with slower velocity than the bulk wave velocity can be used [20].

In our case, focusing on high sensitivity gravimetric sensing, we aim at maximizing the sensitivity by using a thin guiding layer that can confine the Love mode. Since the Love mode is dispersive, we need to perform a preliminary modeling analysis to estimate the guiding layer thickness and acoustic propagation losses based on the LTO electromechanical coefficients and guiding layer properties, namely density and Young modulus determining the acoustic velocity in the thin organic film and its dielectric permittivity.

In order to achieve this objective, dedicated modeling tools [21], [22] are used to calculate the coupling coefficient and velocity of the shear wave for quartz YXl/36° cut, as well as the pseudo-shear wave for LTO YXl/36° cut. The thickness of a poly-methylmethacrylate (PMMA) polymer layer on top of a metalized layer of gold and aluminum acts as the varying parameter. The results of these simulations are shown in Fig. 1 for strongly coupled LTO (c) and for weakly coupled quartz (b), with gold (dashed lines) or aluminum (solid lines) electrodes, displaying the acoustic velocity (a) and electromechanical coupling coefficient (b, c) as a function of PMMA guiding layer thickness. The full set of simulation is shown in the Supplementary material, with additional electrode thicknesses representative of classical cleanroom manufacturing techniques. All devices considered in this investigation have been designed to operate at 155 MHz, so that a wavelength of 26.5 μm is selected for LTO devices and 32.0 μm for quartz devices. All electrodes are split finger with a metallization ratio of 50%. The tunable variables are the guiding layer thickness and the type of metal coating on the sensing area.

The thicknesses of aluminum thin films used for patterning the IDTs have a low impact on both the coupling coefficient and wave velocity variation (Supplementary material, Fig. S1), compared to gold. Gold has a stronger impact on the initial coupling factor when the guiding layer thickness is thin, especially on quartz. This observation can be explained by the mass loading and the softness of gold compared to aluminum. The tradeoff is hence between selecting a chemically inert

Highlights

- **Using a high permittivity piezoelectric substrate – lithium tantalate oxide – for package-less sensing in liquid.**
- **Gravimetric sensitivity assessment of lithium tantalate oxide Love mode surface acoustic wave sensor with respect to quartz depending on guiding layer and electrode properties.**
- **Experimental demonstration of the sensitivity and biosensing applications, including a reflective delay line sensor geometry compatible with wireless sensing.**

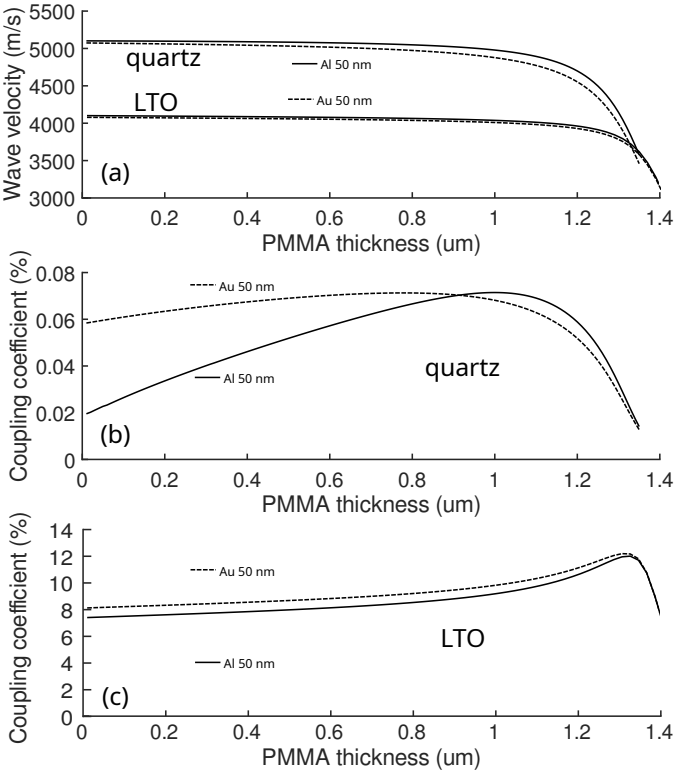

Fig. 1. Comparison of the wave velocity (top) and electromechanical coupling coefficient (middle and bottom) of the shear wave for different thicknesses of the guiding layer in PMMA and for different materials of the metalized surface – Al as solid lines and Au as dashed lines – of lithium tantalate YXl/36° cut and quartz YXl/36° cut as indicated next to each set of curves.

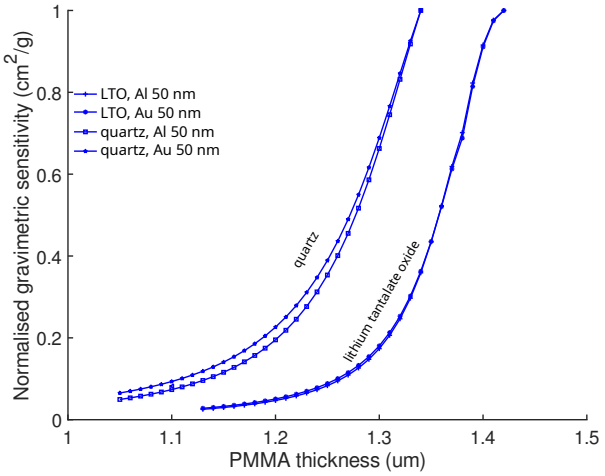

Fig. 2. Dependence of the gravimetric sensitivity for quartz and LTO based SAW devices as a function of the guiding layer thickness for electrodes made either of aluminum or gold.

electrode material, gold, which might impact the acoustic wave properties, or an electrode material with acoustic properties closer to those of the substrates, aluminum, but with chemical reactivity with some compounds in water.

For a quartz substrate, the wave velocity and coupling factors are not computed for a guiding layer thicker than 1.36 μm, or 6.8% of the wavelength. This is due to the electromechanical coupling coefficient becoming too low to be representative of a usable device (Supplementary material S, Fig S2.)

The gravimetric sensitivity S is defined as the normalized frequency variation Δf, due to mass adsorption on the SAW acoustic path acting as the sensing area, to the operating frequency f_0 as a function of mass surface density as (1). This can be written as

$$S = \frac{\Delta f}{f_0} \times \frac{A}{\Delta m} \tag{1}$$

where A is the sensing area and Δm is the adsorbed mass variation. Since $\Delta m = A\rho\Delta h$, where $\rho = 1.185$ g/cm^3 [23] is the adsorbed layer density and Δh is its thickness variation, the Eq. 1 for gravimetric sensitivity can be simplified to

$$S = \frac{\Delta f}{f_0} \times \frac{1}{\rho \times \Delta h} \tag{2}$$

Considering the acoustic velocity $v = \lambda \times f_0$, Eq. 2 becomes

$$S = \frac{\Delta v}{v_0} \times \frac{1}{\rho \times \Delta h} \tag{3}$$

where $\frac{\Delta v}{v_0}$ is the relative velocity variation.

The maximum gravimetric sensitivity is identified as the fastest change in velocity Δv with respect to the guiding layer thickness Δh. Through numerical analysis, the optimal guiding layer thickness for maximizing sensitivity is found to be 1.43 μm for LTO and 1.35 μ for quartz (Fig. 2). The sensitivity primarily relies on the guiding layer thickness and is only marginally influenced by the piezoelectric substrate. Fig. 2 ephasizes the minute impact, in this transmission delay line configuration, of the electrode thickness or material except for the thickest gold layer (150 nm, Supplementary material, Fig. S3) on quartz, since all dispersion curves for a given substrate overlap within numerical uncertainties.

However, the electromechanical coupling coefficient is strongly affected by the thickness of the guiding layer and the selected piezoelectric substrate (Supplementary material S, Fig S2.) as shown on Fig. 1 (b, c). This electromechanical coupling coefficient determines the usability of the device

through the measurement signal to noise ratio, as the electrical signal rises with increasing electromechanical coupling coefficient for a given noise level. Therefore, experimental measurements are conducted to select the optimal thickness of the guiding layer, striking a balance between maximizing sensitivity and maintaining a strong coupling coefficient for a strong transmission S_{21} coefficient. To ensure consistent interpretation of experimental results, only aluminum is used as the metalization layer when fabricating the acoustic path and IDTs.

III. Experimental Results: Sensitivity and Transmission Coefficient

To determine the gravimetric sensitivity based on wave velocity calculation, transmission delay lines are designed and manufactured.

A square chip measuring 16 mm in length contains 4 transmission delay lines (Fig. 3), spin coated with different polymers of varying thicknesses. The distance d between the middle of the two IDTs defines the path length. For the quartz-based delay lines, this distance is 9.0 mm, while for the LTO devices, it is 6.3 mm. The distance is dependent on the number of electrodes in the IDTs, which is selected based on the inverse of the electromechanical coupling coefficient K^2 [24]. The length of the sensing area, without any electrodes, remains constant across all designs. Therefore, LTO with a strong electromechanical coupling coefficient ($K^2 = 10\%$) only requires 20 electrode pairs, whereas the quartz with a weak electromechanical coupling coefficient ($K^2 \simeq 0.06\%$) requires 100 electrode pairs to efficiently launch an acoustic wave.

During the fabrication and measurement of LTO delay lines, a challenge arose in the form of notches in the frequency domain transmission sinc shaped transfer function or in the time-domain echoes. These notches are caused by the pseudo-shear wave generated on the LTO substrate. When the surface wave guided by the thin film converts to a Love mode or when there is metalization between IDT and echoes, the wave slows down and becomes confined to the substrate surface. At the same time, a bulk wave radiates towards the opposite flat side of the device. Since the wavevectors along the propagation direction are the same for the surface and bulk wave, interference between the two waves occurs at the reception IDTs. This interference pattern creates notches in the transfer function where destructive summation of vectors occurs. Mechanical depolishing of the backside of the substrates on which the devices were patterned eliminated this effect and removed the notch in the transfer function (Fig. 4).

The wave velocity, denoted as v, is determined by dividing the known distance between the IDTs d by the phase slope s measured in degrees per Hz as a function of frequency [25] of the transmission coefficient S_{21},

$$c = 360 \times \frac{d}{s} \tag{4}$$

The velocity is measured within the bandpass of the acoustic transducer. It is measured both before and after polymer spin coating, and the difference in measurements is taken into account when plotting the variation in wave velocity with polymer thickness.

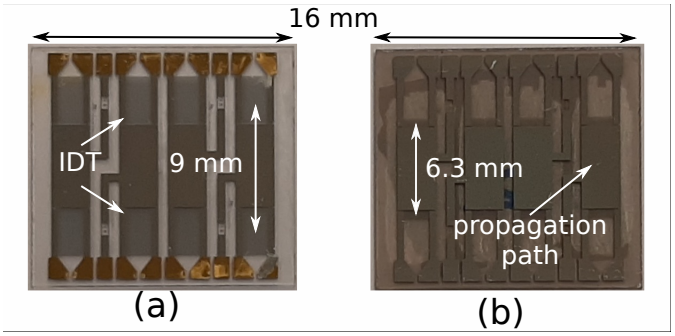

Fig. 3. 16 mm square chip including 4 delay lines patterned on (a) quartz and (b) LTO. The distance between the IDTs is (a) 9 and (b) 6.3 mm, respectively, depending on the number of IDT with 100 electrode pairs for the quartz device and 20 electrode pairs for the LTO device.

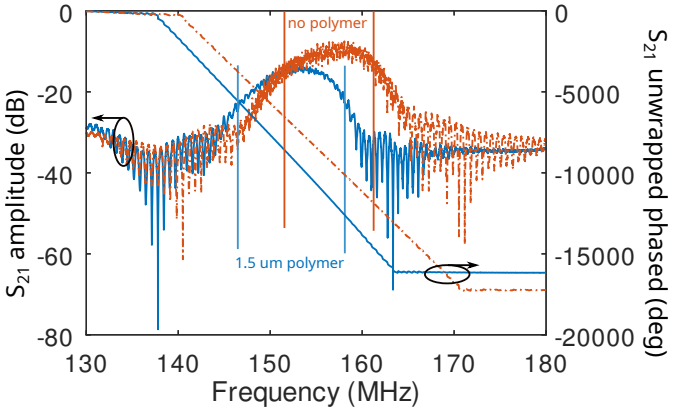

Fig. 4. S_{21} amplitude and phase for a LTO delay line not coated (red) and coated (blue) with a 1.5 μm thick polymer layer. The solid vertical lines indicate the frequency range considered for the phase slope calculation within the band pass of each delay line.

Figure 4 (a) shows the insertion loss measured as the S_{21} amplitude, while Fig. 4 (b) shows the phase. Both measurements are taken before and after polymer deposition. The frequency range used for calculating the phase slope is chosen individually to be in the middle of the bandpass of the delay line, as indicated by the dotted vertical lines.

Two methods are used to achieve different thicknesses of polymer. One is by changing the rotation speed of the spin coater, and the other is by diluting the polymer solution. The combination of acceleration and rotation speed affects the evenness of the polymer layer. To ensure this, the rotation speed is limited to a range of 2500 to 4000 rotations per minute (rpm), with a fixed acceleration of 3500 rpm/s, except for the most viscous solution. During the spin-coating process, the polymer is dispensed at 500 rpm for 30 seconds, with an acceleration of 100 rpm/s, and then the final rotation speed is reached with an acceleration of 500 rpm/s for a duration of 20 seconds.

For spin coating different thicknesses, there are various dilutions of Shipley S18 photoresist available, namely S1805, S1813, and S1828. The deposition parameters are adjusted to achieve the desired thicknesses. For MicroChem SU8

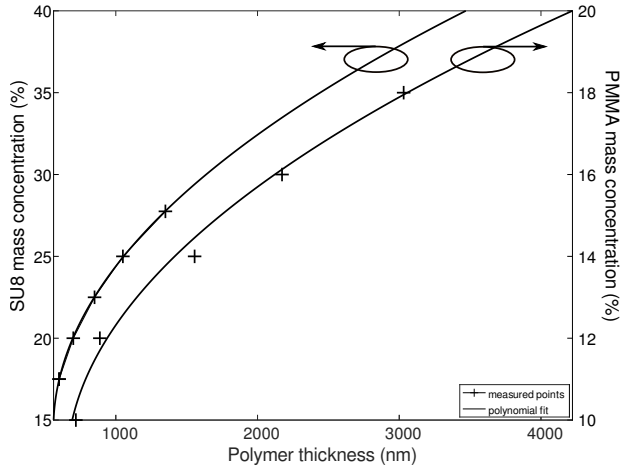

Fig. 5. Mass concentration of SU8 and PMMA for a given thickness obtained on $\mathbf{16}$ mm $\times$ $\mathbf{16}$ mm LTO substrates with the following spin coating parameters: 3500 rpm/s acceleration, 3000 rpm rotation speed for 30 s for SU8 and PMMA with mass concentrations below 16%. For PMMA mass concentrations of 16% and 18%, the high viscosity requires a dispensing protocol with 500 rpm during 30 s with an acceleration of 100 rpm/s before reaching 3000 rpm rotation speed with an acceleration of 500 rpm/s. Crosses (+) are measurements, the solid lines are second order polynomial fits.

epoxy, there is only one solution available, SU8-2010, with a polymer mass concentration of 58%. This solution is diluted in cyclopenthanol solvent to obtain different viscosities and, consequently, different spin-coated thicknesses. PMMA is in a solid state and is dissolved in anisole.

Figure 5 shows the relationship between the mass concentration of SU8 and PMMA and the resulting polymer thickness after spin coating on LTO substrates measuring 16 mm by 16 mm. The second order polynomial fits (solid lines) are used to interpolate the experimental measurements (crosses) and select the appropriate mass concentration to reach a targeted thickness.

After spincoating, SU8 is baked for 2 minutes at 95^{o}C and then exposed to UV at 500 mJ/cm^2, PMMA is baked at 150°C for a duration of 2 minutes, and S1813 is baked for 2 minutes at 120^{o}C. Due to the strong pyroelectricity of LTO, each temperature is reached with a ramp of 20^{o}C per minute to prevent damaging the SAW devices.

Since the final application involves measuring in liquid environments, the optimized thicknesses are selected to have acceptable losses of no more than -25 dB on the S_{21} amplitude measurement. This selection is based on previous studies [26], [27], which showed that protecting the interdigitated transducers with a microfluidic channel leads to a drop in S_{21} amplitude by 20 to 30 dB due to the packaging over the acoustic path. To prevent such losses, LTO is chosen as the substrate, and the threshold of -25 dB is selected for both LTO and quartz substrates.

IV. Measurement results: gravimetric sensitivity

The gravimetric sensitivity measurements are presented after S18 photorestist has been spin coated on both quartz and LTO substrates, which are YXl/36° cut delay lines propagating

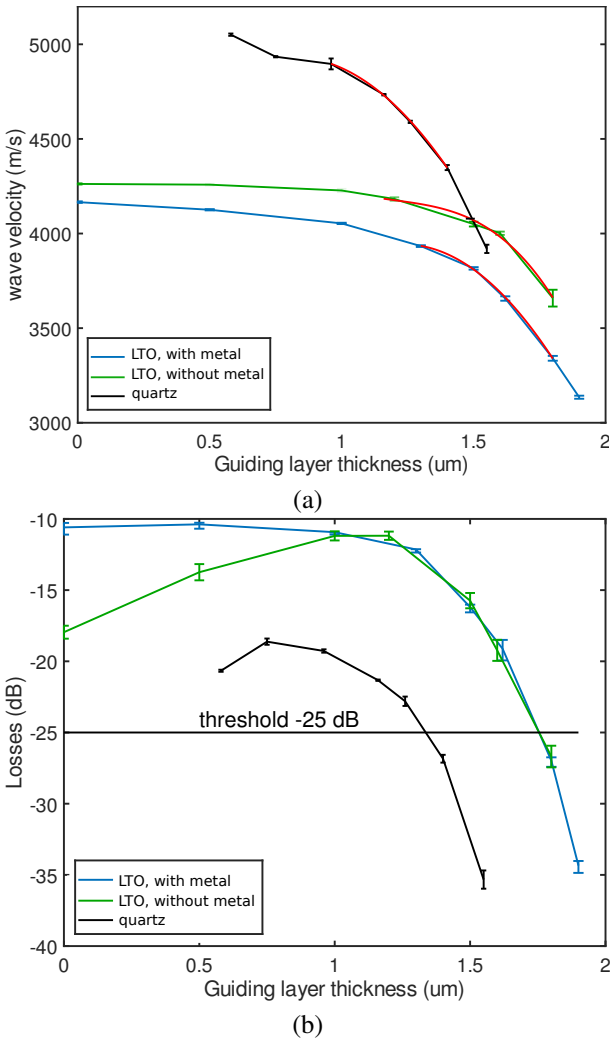

Fig. 6. Wave velocity (a) and maximum of amplitude (b) of S_{21} response for quartz (black) and LTO (green bare LTO surface, blue metallized LTO surface) delay lines as a function of S18 guiding layer thickness. The acoustic velocities (a) are fitted with a second order polynomial fit (red lines) for the determination of the gravimetric sensitivity.

shear waves. The variation of wave velocity with polymer thickness is shown in Fig. 6 (a) for both substrates. The polynomial fit of the velocity for different thicknesses is determined, so that the gravimetric sensitivity is calculated based on a thickness variation obtained as the derivate (difference of adjacent samples) of the polynomial fit and assuming a polymer density of 0.9 g/cm^3. The calculated values are summarized in Tab. I.

The analysis of Fig. 6 (b) shows that the optimal thickness of the polymer is 1.34 μm for quartz and 1.75 μm for LTO when operating at a frequency 155 MHz, selected as the maximum thickness allowing to maximize the sensitivity while keeping losses below the 25 dB threshold. The estimated sensitivities for these optimal thicknesses are approximately 4600 and 6500 cm^2/g for quartz and LTO delay lines, respectively. While these values are higher than those reported in the literature [2], we attribute this strong energy confinemnt to the use of organic polymer guiding layers rather than silicon dioxide, regardless of the nature of the piezoelectric substrate.

TABLE I

VELOCITY v_0 FOR A GIVEN MEASURED POLYMER THICKNESS h AND THE CORRESPONDING GRAVIMETRIC SENSITIVITY S BASED ON THE POLYNOMIAL FIT DEPICTED IN FIGURE 6 (A).

ine substrate	h (μm)	v_0 (m/s)	S (cm^2/g)
ine	1.01	4871.5	1632
	1.07	4820.6	2181
quartz	1.14	4754.3	2751
	1.21	4672.0	3351
	1.27	4574.7	3983
	1.34	4462.1	4658
ine	1.31	3931.6	1037
	1.40	3891.7	2020
lithium	1.49	3822.8	2990
tantalate	1.57	3724.9	4056
	1.66	3598.0	5221
	1.75	3442.2	6526
ine			

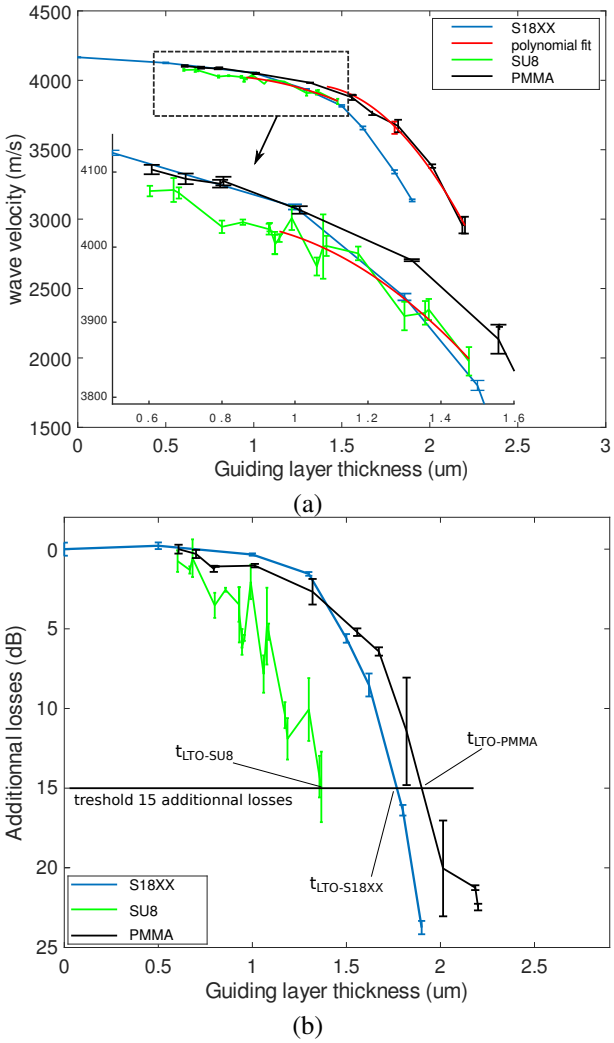

Fig. 7. (a) Variation of maximum of amplitude of S_{21} response and (b) wave velocity of LTO delay lines coated with S18 (blue), SU8 (green) photoresists and PMMA (black). (a) second degree polynomial fit (red solid lines) of the curve for the determination of the gravimetric sensitivity. The inset zooms on the part of the curve relevant to the acceptable insertion losses.

Notice how the pseudo-shear wave propagated on LTO induces significant losses when the acoustic path between IDTs is neither metallized nor coated with a guiding layer to prevent the surface wave from radiating in the bulk of the piezoelectric substrate (Fig. 6, green curve on the left of chart (b) exibiting up to 18 dB losses), emphasizing the need to either metallize or convert the pseudo-shear wave to a Love wave with the guiding layer to slow the surface wave below the velocity of the bulk wave and prevent radiation into the bulk.

Using the same process, SU8 photoresist and PMMA polymer are spin coated on LTO delay lines. The additional losses on the maximum amplitude of the S_{21} measurement are shown in Fig. 7 (a), and the wave velocity is shown in Fig. 7 (b). Assuming an initial -10 dB maximum amplitude without polymer coating, Figs. 4 and 6 (b) aim to identify a polymer coating that introduces a maximum of 15 dB additional losses, respectively. Therefore, the optimal thickness for the SU8 photoresist guiding layer $t_{LTO-SU8}$ is determined to be 1.4 μm, while for PMMA $t_{LTO-PMMA}$ it is 1.95 μm. The difference between these results and the S18 photoresist results is due to the mechanical properties of the thin polymer films.

The gravimetric sensitivity for S18 photoresist on quartz and LTO delay lines is calculated for thicknesses ranging from 75% of the optimal thickness to the optimal thickness as shown in Fig. 7. The corresponding gravimetric sensitivities are calculated using a density of 1.22 g/cm^3 for SU8 and 1.185 g/cm^3 for PMMA, and shown in Fig. 8: the optimal thickness leading to additional losses lower than 15 dB are identified as $t_{LTO-SU8} \simeq 1.4$ μm for SU8 and $t_{LTO-S18XX} \simeq 1.8$ μm for S18XX photo-resists, and $t_{LTO-PMMA} \simeq 1.95$ μm for PMMA.

The gravimetric sensitivity obtained with a SU8 guiding layer on LTO ranges from 400 to 1000 cm^2/g. This is lower than the sensitivity range achieved with S18 photoresist (1000 to 6500 cm^2/g) and PMMA (900 to 4200 cm^2/g). The poor sensitivity with SU8 coating is attributed to the stiff epoxy layer with poorer energy confinement capability than the slower PMMA and S18 whose strong mismatch with the piezoelectric substrate surface acoustic wave velocity leads to efficient Love mode conversion and energy trapping close to the surface. PMMA allows for thicker guiding layers compared to SU8 and S18 thanks to lower propagation losses. Although the gravimetric sensitivity of PMMA is lower than that of S18, it remains a good candidate for a guiding layer because of its chemical stability to the environment leading to a stable reference baseline.

This experimental section is now concluded with a comparison with the modeling results from section II. Figure 1 exhibited a sharp drop in the acoustic velocity as a function of guiding layer thickness of 1.3 to 1.4 μm which resulted, as shown in Fig. 2, in a maximum sensitivity at such guiding layer thicknesses since the adlayer acts as a parturbative addition to the guiding layer thickness. These results match the experimental measurements of Fig. 6 (a) where the velocity starts collapsing at guiding layer thicknesses of 1.3 to 1.4 μm. Furthermore, the signal transmitted in quartz devices (Fig. 6 (b)) are weaker by 10 dB with respect to LTO delay lines, in qualitative agreement with the 100-times weaker electromechanical coupling coefficient of the former

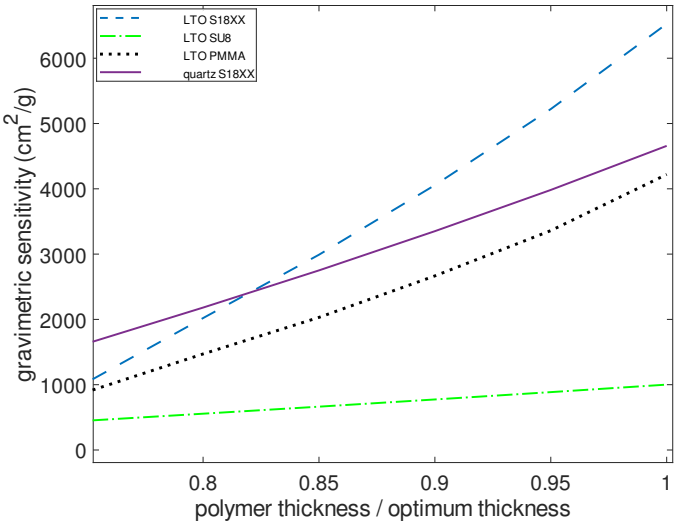

Fig. 8. Gravimetric sensitivity as a function of the guiding layer thickness over the optimum thickness for LTO delay line coated with S18 photoresist (blue dashed lines), SU8 (green dash-dot line) and PMMA (black dotted lines), and for quartz delay line (purple solid line) coated with S18 photoresist.

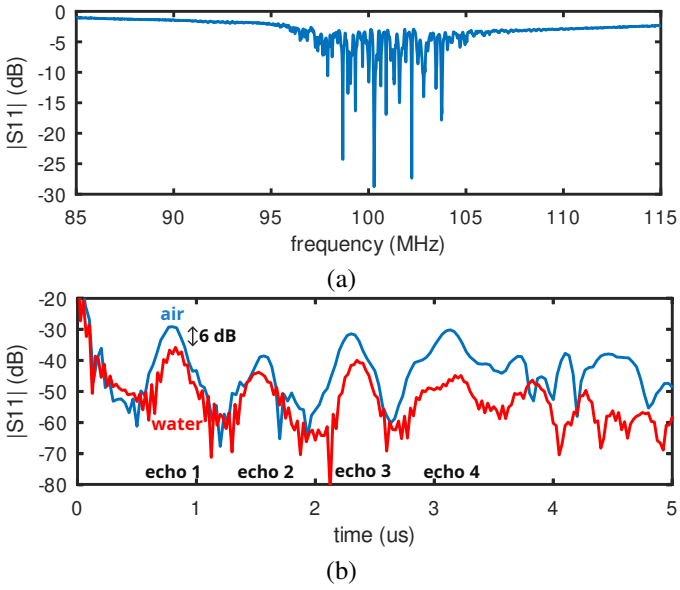

Fig. 9. (a) Frequency domain response of the reflective delay line designed with four echoes. (b) Inverse Fourier transform of the frequency-domain response to recover the time-domain response, with the 4 echoes clearly seen at $N \times 0.8\ \mu$s, $N \in [1:4]$. The delay of $0.8\ \mu$s is selected as a tradeoff between recording the sensor response beyond clutter on the one hand, and limiting the maximum delay and hence path length to $5\ \mu$s on the other hand. On the bottom chart, the blue curve was collected in air, and the red curve while dipping the sensor in deionized water with no fluidic protection on the acoustic path, the IDT or the wire bonding. Insertion losses are observed to only rise by 6 dB when dipping the sensor in water.

with respect to the latter. The peak transmitted power for quartz is observed when the guiding layer is 1 μm as predicted from modeling. Since the effective electromechanical coupling coefficient is a combination of intrinsic piezoelectric substrate electromechanical coefficient and geometrical layout of the IDTs, the quantitative match on the power ratio is not expected from the 1-dimensional modeling which does not account for electrode geometries but only considers plane waves propagating on flat interfaces. Hence, modeling has driven the design considerations of the fabricated devices whose behaviour matches the predicted characteristics.

While the gravimetric sensitivity analysis focused on transmission delay lines for ease of interpretation, the ultimate goal of this research is to achieve wireless passive sensing of chemical compounds in liquid phase [28]. These preliminary results have led to the development of a reflective delay line and its use in a biosensing application: unlike past similar research [29], we focus here on pure shear wave propagation on a high permittivity substrate for in-situ package-less wireless detection of (bio)chemical compounds in water.

V. Reflective Delay Line

A. Design considerations

This section deals with the application of detecting pollutant in the sub-surface water table. Considering GPR [28] as a classical geophysical measurement tool, a Love-mode reflective acoustic delay line is designed as cooperative target returning an echo with a delay dependent on the pollutant concentration. Since this discussion focuses exclusively on the sensing element of the transducer, we do not address the connection of the piezoelectric die to the antenna nor the design considerations of this antenna. Past investigations [30] have shown how a bowtie antenna is a robust candidate for collecting the incoming electric field radiated by the GPR and polarizing the SAW sensor IDTs to generate the acoustic wave.

In a wireless sensing application, a single antenna is used to collect electromagnetic waves and polarize the IDT on a transducer. The electromagnetic energy is then converted to an acoustic wave using the inverse piezoelectric effect of the substrate. This acoustic wave propagates as a surface wave when suitable substrate cut and guiding layers are chosen.

The insertion losses of the time-domain echoes of the LTO delay line can be seen in Fig. 9 in the frequency domain response (top) and time domain response (bottom) generated by taking the magnitude of the inverse Fourier transform of the frequency domain response. These losses exhibit a drop of less than 3 dB when the delay line is immersed in deionized water without any protection on the acoustic path, IDT, or wire bonding (Fig. 9).

The range of the frequency domain is determined by the mechanical period of the IDT for the center frequency and the electromechanical coupling coefficient of the piezoelectric substrate for the span. The number of collected samples in the frequency domain, and therefore in the time domain, is determined by the longest echo delay. In this case, a center frequency of 100 MHz or 200 MHz (41 and 20.5 μm wavelength respectively) and a span of 20 MHz are chosen to be compatible with commercial off-the-shelf GPR for passive wireless subsurface pollutant detection. This results in a timestep of 50 ns after the inverse Fourier transform, with 100 samples being sufficient to cover the time-domain range of 0 to 5 μs determined by the longest IDT to Bragg mirror acoustic path length and the acoustic velocity.

The transmission delay line has been expanded to a reflective delay line architecture for wireless sensing applications. In a reflective delay line, Bragg mirrors are patterned on the substrate to reflect the acoustic energy back to the same IDT connected to the antenna. These Bragg mirrors serve as another degree of freedom and are designed as Bragg reflectors with periodically patterned electrodes. Each electrode acts as a reflector due to the mismatch between the metallized and free acoustic velocity, leading to a reflection coefficient. By spacing the electrodes every half wavelength, the reflected energy accumulates constructively. The reflection coefficient can be adjusted by selecting the number of electrodes in each Bragg mirror. In the proposed design, all Bragg mirrors are made of 80 electrodes spaced by half-wavelength with a metallization ration of 50%, leading to the weak response of echo 2 since this Bragg mirror is located after the Bragg mirror generating echo 1, as seen on Fig. 9. Replacing the second IDT with Bragg mirrors separated by different path lengths from the unique IDT connected to the antenna allows for patterning multiple Bragg mirrors on both sides of the transducer. Thanks to the different path lengths from IDT to each Bragg mirror, the returned echoes are received with different delay, allowing for a differential measurement on a single device. By using local chemical functionalization between each Bragg mirror, the sensor range contribution to the interrogation unit (GPR) can be subtracted through a differential analysis during post-processing of the collected data, in which one echo delay acts as a reference which is subtracted from all other delays. If the path between IDT and this reference echo is free of chemical functionalization, its delay is solely determined by the distance between the GPR and the sensor and to the piezoelectric substrate acoustic velocity with its dependence to temperature or stress. The subtraction of this reference delay to all other echo delays cancels these common effects and allows extracting only the impact of the chemical reaction to the guiding layer acoustic velocity through mass loading (decrease in velocity) or stiffening (increase of velocity).

Moreover, the electrodes can either be left as floating potential, relying solely on mechanical reflection, or configured as IDTs to function as re-emission sources when an electric field is generated by the electromechanical conversion of the incoming acoustic wave. The first geometry implements a reflective behavior where the acoustic velocity mismatch between free space and metalized space causes the wave to reflect and interfere constructively back towards the IDT in a Bragg mirror configuration. The second is a re-emission geometry where the current generated in the Bragg mirror itself polarizes the substrate, creating a new acoustic wave at the Bragg mirror location. In the former case, all electrodes are either short circuited or floating, while in the latter case, the electrodes are connected in an IDT geometry. In the latter case, the interdigitated transducers on the piezoelectric substrate are either apodized or uniformly weighted, with a short length of electrode on the busbar to avoid transverse modes in the strongly coupled piezoelectric substrate. The latter architecture was chosen for strongly coupled LTO devices when designing the reflective delay lines. Figure 10 provides a visual representation of the sensor. The economical viability of the design is emphasized with 21 devices manufactured with each processed 4"-wafer, each device comprising 4 channels or a total of 84 sensors.

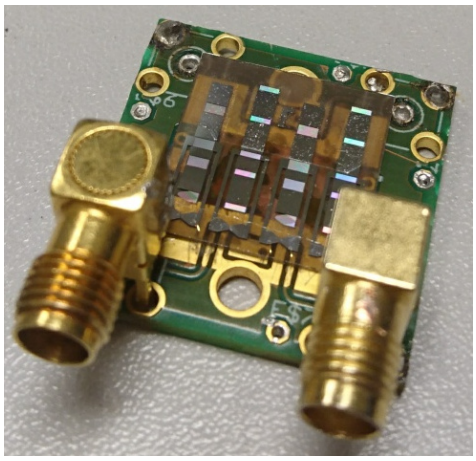

Fig. 10. Acoustic sensor assembled on a printed circuit board and ready for use for sensing in water. On this layout, both 100 MHz (left and third from left) and 200 MHz (second and fourth from left) are dupplicated for reproducibility assessment. It was observed that Bragg mirrors evenly distributed at $N \times \tau$ with $N \in [1:4]$ and τ arbitrarily set to 0.8 μs to allow clutter to fade out while limiting acoustic propagation losses led to optimal measurement conditions. Notice the lack of microfluidic element on the acoustic path since water is allowed to reach the IDTs. See Fig. 11 for a usage demonstration.

B. Time domain measurement setup and procedure

Reflective delay lines are used in sensor technology by delaying echoes in the time domain. The duration of the delay is determined by twice the distance from the IDT to the Bragg mirror, divided by the acoustic velocity. This means that if the wave is slower, for example due to mass loading, the delay introduced by the wave propagating on the surface of the sensor will be longer. These sensors are designed to be compatible with pulsed-mode time-domain GPR measurements, which allow for fine time of flight delay measurement [31]. However, in laboratory experiments, a vector network analyzer (VNA) is used for frequency domain measurements. The resulting data is then interpreted in the time domain through an inverse Fourier transform.

Because the Fourier transform of discrete time samples is periodic, two frequency axis organizations are used by various digital processing software, namely ranging from 0 to the sampling frequency or from the negative Nyquist frequency – half the sampling frequency – to the Nyquist frequency. Matlab, GNU Octave, and Numerical Python `numpy` use the former convention, with the Nyquist frequency located in the middle of the abscissa range. On the other hand, a VNA measurement ranges from the center frequency minus half the span to the center frequency plus half the span. This means that the baseband center frequency is at the center of the abscissa range, spanning from minus half the sampling frequency to half the sampling frequency. Switching between these conventions is a matter of switching the quadrants from minus Nyquist frequency to 0, and from 0 to Nyquist frequency, which is achieved using the `fftshift()` command.

To compute the time domain characteristics, the frequency-dependent scattering reflection coefficient $S_{11}(f)$ is measured, and then

$$S_{11}(t) = \text{ifft}(\text{fftshift}(S_{11}(f)))$$

the inverse Fourier transform is computed to obtain $S_{11}(t)$.

The phase of $S_{11}(t)$ *at a fixed delay*, determined as the point of maximum reflection magnitude, is the measurement of interest. A decrease in velocity due to mass loading will result in a drop in phase.

The phase introduced by a wave at frequency f, propagating at velocity v over a length d, can be expressed as $\varphi(f) = 2\pi f\tau = 2\pi fd/v$. This expression emphasizes the phase increase as the velocity drops at a *fixed frequency* (on the VNA output). However, in the time domain output at the fixed delay τ, the phase at swept frequency f is expressed as $\varphi(\tau) = 2\pi\frac{v}{\lambda}\tau$, where λ is the fixed wavelength determined by the IDT geometry. This expression leads to a *decreasing* phase at a fixed delay τ as the velocity v *decreases*. All measurements conducted in this study show a decreasing phase at a fixed delay, indicating mass loading. This occurs when the analyte being studied absorbs into the sensing surface and causes a decrease in the acoustic wave velocity.

VI. Experimental Results: Biosensing

To demonstrate the usability of the proposed device, we tested a LTO reflective delay line with no specific surface functionalizion beyond the polymer guiding layer. We exposed it to proteins from dehydrated milk in a phosphate buffer saline (PBS) solution. The goal of the experiment was to see if we could recover the phase from multiple echoes of the delay line when proteins non-specifically adsorb to the surface. This is a traditional method for saturating the free areas of a functionalized biosensor surface (Fig. 11). To create the protein solution, we mixed 50 mg of dehydrated milk with 100 ml of PBS. We observed a stable baseline after removing any thermal drift, and then we injected and mixed in the dehydrated milk. This caused the non-specific adsorption of proteins to start at date 1000 on our timeline. Recording continued until an asymptotic behavior was reached, indicating the formation of a stable protein film on the sensing area.

The echoes identified with integer index $i > 0$ at different delays τ_i, ranging from 0.8 to 3.2 μs, exhibit a phase shift proportional to the adsorbed mass and their respective delays. The phase shift is calculated using the formula $\varphi_i = 2\pi f\tau_i = 2\pi\frac{v}{\lambda}\tau_i \propto v \times i$, where $f = 200$ MHz is the center frequency of the IDTs, and $\tau_i = d_i/v$ represents the travel time from IDT to Bragg mirror and back to IDT. The acoustic velocity, v, varies when the sensing surface is exposed to the substance being detected.

In the case of a thinner guiding layer selected to lower the insertion losses, when the gravimetric sensitivity, S, is approximately 1000 cm^2/g (Fig. 8 for the experimental determination of this value), the measurement in Fig. 11 is analyzed as follows:

1) The shortest echo, with a delay of 0.8 μs, causes a phase rotation of $\varphi_1 = 360 \times 0.8 \times 200 = 57600°$ at the center frequency of 200 MHz.

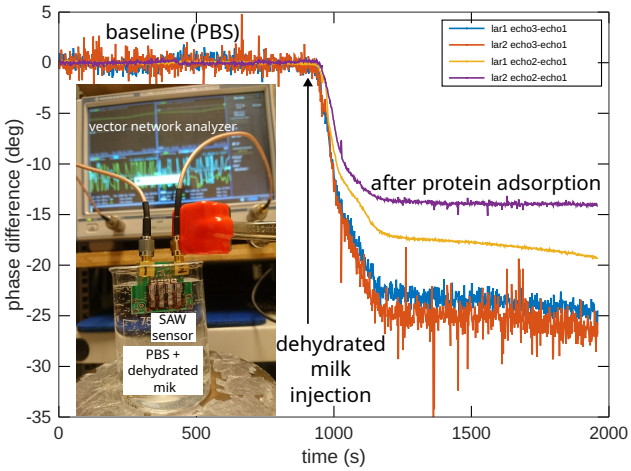

Fig. 11. Response of the four echoes patterned on a reflective SAW delay line upon exposure to a high concentration of immunoglobins from dehydrated milk in phosphate buffer saline (PBS) solution injected a 1000 s following a PBS baseline stabilization. Inset: picture of the experimental setup, emphasizing the lack of dedicated microfluidic handling elements on the acoustic path.

2) The observed phase rotation of approximately 15° is interpreted as mass loading due to an adsorbed protein thin film with a mass density of $\frac{dm}{A} = \frac{1}{S} \times \frac{d\varphi}{\varphi} \simeq 260$ ng/cm^2. This is a reasonable estimate for non-specific binding in a saturated dehydrated milk solution dissolved in phosphate buffer solution (PBS) as was discussed earlier [32] when estimating that a densely packed layer of immunoglobulin proteins would weight 200 to 550 ng/cm^2 depending on the selected protein characteristics.

Assuming the protein film is similar to a polymer thin film with a density of around 1.5 g/cm^3, the characteristics of this layer suggest it is a 0.2 μm thick adsorbed film. This film acts as a perturbation to the initial guiding layer according to Fig. 6, and it demonstrates the occurrence of a multilayer physisorption.

Using a vector network analyzer (VNA) allows for precise measurement of the phase with sub-degree accuracy. The differential measurement, subtracting the phase of multiple echoes, cancels out correlated effects such as range to the reader electronics, temperature, and hydrostatic pressure. With a phase measurement resolution of $d\varphi = 1°$, the detection limit at $S = 1000$ cm^2/g is $\frac{dm}{A} \simeq 15$ ng/cm^2.

VII. Conclusion

Transmission and reflective delay lines made from lithium tantalate have been specifically engineered to address the challenges posed by capacitive short-circuit between interdigitated electrodes when exposed to liquids with a high permittivity like water. This coupling typically leads to excessive insertion losses in the acoustic response. The resulting designs, which propagate a pseudo-shear wave, are compatible with surface energy confinement when guided in a thin polymer film, acting as a Love mode conversion layer.

These designs have been demonstrated to function effectively for liquid-phase measurements, even under conditions of high ionic concentration such as in a phosphate buffer saline

solution. Notably, there is no need for a dedicated microfluidic system to prevent the liquid from reaching critical components of the surface acoustic wave transducer, as would be necessary for low permittivity substrates. This achievement paves the way for the implementation of lithium tantalate as a potent piezoelectric material for sensing in water, addressing a significant challenge in biosciences and environmental sciences.

REFERENCES

[1] E. Gizeli, *Acoustic transducers*, E. Gizeli and C. R. Lowe, Eds. CRC Press, 2002.

[2] L. A. Francis, J.-M. Friedt, C. Bartic, and A. Campitelli, "An SU-8 liquid cell for surface acoustic wave biosensors," in *MEMS, MOEMS, and Micromachining*, vol. 5455. SPIE, 2004, pp. 353–363.

[3] M.-I. Rocha-Gaso, J.-V. García, P. García, C. March-Iborra, Y. Jiménez, L.-A. Francis, Á. Montoya, and A. Arnau, "Love wave immunosensor for the detection of carbaryl pesticide," *Sensors*, vol. 14, no. 9, pp. 16 434–16 453, 2014.

[4] M. I. Rocha Gaso, "Analysis, implementation and validation of a Love mode surface acoustic wave device for its application as sensor of biological processes in liquid media," Ph.D. dissertation, Editorial Universitat Politècnica de València, 2013.

[5] L. El Fissi, J.-M. Friedt, F. Cherioux, V. Luzet, and S. Ballandras, "Fabrication and packaging technologies of Love-wave-based microbalance for fluid analysis," *Sensors and Actuators A: Physical*, vol. 162, no. 2, pp. 304–309, 2010.

[6] K. Mitsakakis, A. Tserepi, and E. Gizeli, "Integration of microfluidics with a Love wave sensor for the fabrication of a multisample analytical microdevice," *Journal of Microelectromechanical Systems*, vol. 17, no. 4, pp. 1010–1019, 2008.

[7] A. Samarentsis, A. Pantazis, A. Tsortos, J.-M. Friedt, and E. Gizeli, "Hybrid sensor device for simultaneous surface plasmon resonance and surface acoustic wave measurements," *Sensors*, vol. 20, no. 21, p. 6177, 2020.

[8] D. Ballantine Jr, R. M. White, S. J. Martin, A. J. Ricco, E. Zellers, G. Frye, and H. Wohltjen, *Acoustic wave sensors: theory, design and physico-chemical applications*. Elsevier, 1996.

[9] K. K. Zadeh, A. Trinchi, W. Wlodarski, and A. Holland, "A novel Love-mode device based on a Zno/ST-cut quartz crystal structure for sensing applications," *Sensors and Actuators A: Physical*, vol. 100, no. 2-3, pp. 135–143, 2002.

[10] M. J. Vellekoop, "Acoustic wave sensors and their technology," *Ultrasonics*, vol. 36, no. 1-5, pp. 7–14, 1998.

[11] G. Kovacs and A. Venema, "Theoretical comparison of sensitivities of acoustic shear wave modes for (bio) chemical sensing in liquids," *Applied Physics Letters*, vol. 61, no. 6, pp. 639–641, 1992.

[12] G. McHale, M. Newton, and F. Martin, "Theoretical mass sensitivity of Love wave and layer guided acoustic plate mode sensors," *Journal of Applied Physics*, vol. 91, no. 12, pp. 9701–9710, 2002.

[13] F. Höök and B. Kasemo, "The QCM-D technique for probing biomacromolecular recognition reactions," *Piezoelectric sensors*, pp. 425–447, 2007.

[14] D. Rabus, J.-M. Friedt, S. Ballandras, T. Baron, É. Lebrasseur, and É. Carry, "High-overtone bulk-acoustic resonator gravimetric sensitivity: Towards wideband acoustic spectroscopy," *Journal of Applied Physics*, vol. 118, no. 11, 2015.

[15] L. Cervera-Chiner, M. Juan-Borrás, C. March, A. Arnau, I. Escriche, Á. Montoya, and Y. Jiménez, "High fundamental frequency quartz crystal microbalance (hff-qcm) immunosensor for pesticide detection in honey," *Food Control*, vol. 92, pp. 1–6, 2018.

[16] K. R. Ross and L. A. Todd, "Field evaluation of a transportable open-path FTIR spectrometer for real-time air monitoring," *Applied occupational and environmental hygiene*, vol. 17, no. 2, pp. 131–143, 2002.

[17] K. Soga, C. Kechavarzi, L. Pelecanos, N. de Battista, M. Williamson, C. Y. Gue, V. Di Murro, M. Elshafie, D. Monzón-Hernández Sr, E. Bustos *et al.*, "Fiber-optic underground sensor networks," in *Underground sensing*. Elsevier, 2018, pp. 287–356.

[18] J. Alonso, "Intrinsic fiber optic chemical sensors for subsurface detection of CO_2," Intelligent Optical Systems, Inc., Torrance, CA (United States), Tech. Rep., 2016.

[19] K.-Y. Hashimoto, *Surface acoustic wave devices in telecommunications*. Springer, 2000, vol. 116.

[20] K.-Y. Hashimoto and H. Yamaguchi, "Excitation and propagation of shear-horizontal-type surface and bulk acoustic waves," *IEEE transactions on ultrasonics, ferroelectrics, and frequency control*, vol. 48, no. 5, pp. 1181–1188, 2001.

[21] A. Reinhardt, T. Pastureaud, S. Ballandras, and V. Laude, "Scattering matrix method for modeling acoustic waves in piezoelectric, fluid, and metallic multilayers," *Journal of Applied Physics*, vol. 94, no. 10, pp. 6923–6931, 2003.

[22] S. Ballandras, M. Wilm, W. Daniau, A. Reinhardt, V. Laude, and R. Armati, "Periodic finite element/boundary element modeling of capacitive micromachined ultrasonic transducers," *Journal of Applied Physics*, vol. 97, no. 3, 2005.

[23] J. P. Chung, Y. M. Seong, T. Y. Kim, Y. Choi, T. H. Kim, H. J. Choi, C. H. Min, H. Benmakhlouf, K. J. Chun, and H.-T. Chung, "Development of a PMMA phantom as a practical alternative for quality control of gamma knife® dosimetry," *Radiation Oncology*, vol. 13, pp. 1–9, 2018.

[24] D. Morgan, *Surface acoustic wave filters: With applications to electronic communications and signal processing*. Academic Press, 2010.

[25] G. McHale, F. Martin, and M. Newton, "Mass sensitivity of acoustic wave devices from group and phase velocity measurements," *Journal of Applied Physics*, vol. 92, no. 6, pp. 3368–3373, 2002.

[26] M. Goto, O. Iijima, T. Kogai, and H. Yatsuda, "Point-of-care SH-SAW biosensor," in *2010 IEEE International Ultrasonics Symposium*. IEEE, 2010, pp. 736–739.

[27] G. Papadakis, J.-M. Friedt, M. Eck, D. Rabus, G. Jobst, and E. Gizeli, "Optimized acoustic biochip integrated with microfluidics for biomarkers detection in molecular diagnostics," *Biomedical Microdevices*, vol. 19, pp. 1–11, 2017.

[28] J.-M. Friedt, G. Martin, G. Goavec-Merou, D. Rabus, S. Alzuaga, L. Arapan, M. Sagnard, and E. Carry, "Acoustic transducers as passive cooperative targets for wireless sensing the sub-surface world: challenges of probing with ground penetrating radar," *MDPI Sensors*, vol. 18, no. 1, p. 246, January 2018.

[29] W. Wang and S. He, "A Love wave reflective delay line with polymer guiding layer for wireless sensor application," *Sensors*, vol. 8, no. 12, pp. 7917–7929, 2008.

[30] D. J. Daniels, *Ground penetrating radar*. Iet, 2004, vol. 1.

[31] D. Rabus, L. Arapan, P. Tanguy, J.-M. Friedt, and F. Chérioux, "Sampling frequency fluctuations of the Sensors & Software SPIDAR GPR when probing passive surface aoustic wave delay lines for pollution sensing," *IEEE Geoscience and Remote Sensing Letters*, vol. 19, no. 3503005, pp. 1–5, 2021.

[32] C. Zhou, J.-M. Friedt, A. Angelova, K.-H. Choi, W. Laureyn, F. Frederix, L. A. Francis, A. Campitelli, Y. Engelborghs, and G. Borghs, "Human immunoglobulin adsorption investigated by means of quartz crystal microbalance dissipation, atomic force microscopy, surface acoustic wave, and surface plasmon resonance techniques," *Langmuir*, vol. 20, no. 14, pp. 5870–5878, 2004.